



Mantle heterogeneity and off axis volcanism on young Pacific lithosphere

Nicholas Harmon ^{a,*}, Donald W. Forsyth ^b, Dayanthie S. Weeraratne ^c, Yingjie Yang ^d, Spahr C. Webb ^e

^a University of Southampton, National Oceanography Centre, European Way, Southampton, Hampshire, SO14 3ZH, United Kingdom

^b Brown University, Providence, RI, United States

^c California State University, Northridge, Northridge, CA, United States

^d ARC National Key Centre for Geochemical Evolution and Metallogeny of Continents, Department of Earth and Planetary Sciences, Macquarie University, North Ryde, NSW, Australia

^e Lamont Doherty Earth Observatory, Columbia University, New York, NY, United States

ARTICLE INFO

Article history:

Received 14 July 2011

Received in revised form 8 September 2011

Accepted 22 September 2011

Available online 20 October 2011

Editor: Y. Ricard

Keywords:

MELT

GLIMPSE

East Pacific Rise

marine geophysics

surface wave tomography

small-scale convection

ABSTRACT

Plate tectonics and mantle plumes explain most volcanism on earth, but there are numerous actively forming linear volcanic chains in the middle of tectonic plates that are not explained by these theories. Using the multidisciplinary geophysical dataset of the MELT and GLIMPSE experiments, we show that associated with 3 volcanic chains west of the East Pacific Rise there are low seismic velocities and densities in the asthenosphere that extend to the East Pacific Rise spreading center. Analogous to the Hawaiian swell, the low-density anomalies produce swells beneath the volcanoes on young seafloor. The associated gravity anomalies are part of a set of gravity lineaments that have been previously interpreted as being due to thermo-elastic cracking of the lithosphere or small-scale convection. The correlation between the surface volcanism and subsurface density and velocity anomalies and their extension to the spreading center suggest that pre-existing, buoyant or fertile asthenospheric mantle heterogeneities are stretched in the direction of plate motion by shear between the plate and the underlying mantle. These heterogeneities seed small-scale convection, producing upwelling and pressure release melting, forming volcanic chains that extend nearly to the ridge axis.

© 2011 Elsevier B.V. All rights reserved.

1. Introduction

Volcanism at plate boundaries, such as mid ocean ridges and volcanic arcs, is well explained by decompression melting of upwelling mantle caused by large-scale convection in the earth and melting temperature depression caused by hydration of the mantle wedge due to devolatilization of the subducting slabs. While decompression melting of actively upwelling, hot material explains intraplate hot spots such as Hawaii. Outside of these tectonic settings, particularly in the middle of plate interiors on the ocean floor, significant volcanism is not expected but often observed. Where these volcanoes and seamounts form, alternative models, such as cracking of the lithosphere and tapping ambient asthenospheric melt (e.g. Cormier et al., 2011; Gans et al., 2003; Sandwell and Fialko, 2004) or sublithospheric small-scale convection (Buck and Parmentier, 1986; Haxby and Weisell, 1986), with shallow upwelling and decompression melting, are often invoked to explain the origin of the volcanism. Differentiating between these models is often hampered in the deep ocean basins by the remoteness of the seamounts, yet the origin of the volcanism has important implications for the nature of the asthenosphere and convection in the Earth's interior.

On the Pacific plate there are actively forming linear intraplate volcanic ridges (Winterer and Sandwell, 1987) such as the Puka Puka, Sojourn and Hotu Matua ridge systems that clearly do not have an age progression consistent with formation over a fixed hotspot (Forsyth et al., 2006; Sandwell et al., 1995). Rather, these seamounts in some cases have near synchronous ages over hundreds of kilometers that could be consistent with either rapid, channelized return flow from the Pacific Superswell (Janney et al., 2000; Phipps Morgan et al., 1995; Weeraratne et al., 2003), or hotline volcanism caused by lithospheric cracking (Gans et al., 2003; Sandwell and Fialko, 2004), diffuse extension (Sandwell et al., 1995) or the onset of small-scale convection (Ballmer et al., 2009, 2010). The volcanic chains are linear, comprising seamounts and en echelon ridges of various length, sometimes rising > 1 km above the rest of the seafloor, and extending for hundreds of kilometers (Forsyth et al., 2006; White et al., 2006) or thousands of kilometers, in the case of the Puka Puka ridges (Sandwell et al., 1995).

These volcanic ridges are coincident with an enigmatic basin-wide pattern of banded free air gravity lows and highs on the Pacific plate (Haxby and Weisell, 1986) (Fig. 1) aligned in the direction of absolute plate motion, in some cases cross cutting fossil fracture zones obliquely. The free air gravity lineaments are nearly absent beneath the East Pacific Rise axis, which begin within a hundred kilometers west of the East Pacific Rise (EPR) with amplitudes of 5–10 mGal and wavelengths of 150–200 km, then grow in amplitude to 10–20 mGal and shift to somewhat longer dominant wavelengths further away from the

* Corresponding author.

E-mail address: n.harmon@soton.ac.uk (N. Harmon).

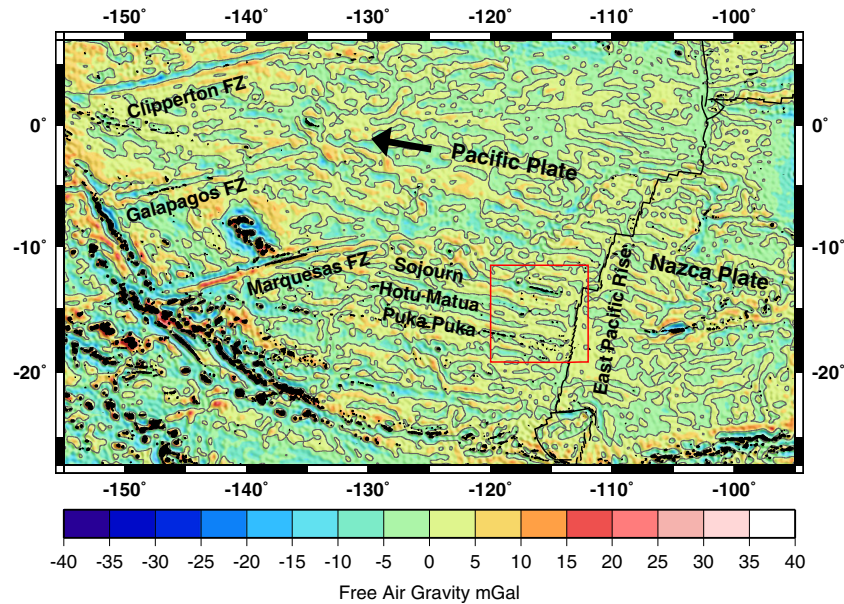


Fig. 1. The band-pass filtered ($50 < \text{wavelength} < 600$ km) free air gravity anomaly from satellite altimetry (Sandwell and Smith, 2009) shows the broad region over which the gravity lineaments exist in the Pacific Ocean. The lineaments exist on the Pacific plate and are less well developed on the Nazca plate. The thick black lines indicate the plate boundaries; black regions indicate areas of seamount volcanism superimposed on the filtered gravity field. The black arrow indicates the direction of absolute plate motion of the Pacific plate in a hotspot reference frame. The red box highlights our study area and encloses the eastern end of the Puka Puka ridge, Sojourn Ridge, and Hotu Matua volcanic complex.

axis, extending westward thousands of kilometers (Haxby and Weissel, 1986; Marquart et al., 1999).

The mantle beneath the Pacific plate near the southern EPR from 5 to 20°S appears to be heterogeneous with respect to temperature, composition and melt, which may contribute to the underlying process that causes the lineaments and intraplate volcanism. For example, subsidence of the Pacific plate from 5°S to the Easter microplate (~23°S) is slower with respect to seafloor age than the adjacent Nazca plate (Cochran, 1986; Forsyth et al., 2006; Scheirer et al., 1998). The variation in subsidence can be explained by higher temperatures beneath the Pacific plate, with a thermal gradient from west to east of 0.05–0.10 °C/km (Cochran, 1986). Higher temperatures beneath the Pacific plate have also been inferred from across-axis resistivity profiles near 17°S on the EPR, which show lower resistivity by up to an order of magnitude beneath the Pacific plate, relative to the Nazca plate in the upper 150 km (Baba et al., 2006a; Evans et al., 2005). The low resistivity may also be consistent with higher water contents at 60–150 km depth in the mantle (Baba et al., 2006a; Evans et al., 2005).

Seismically, there is a pronounced asymmetry across the EPR in the compressional and shear velocity structures of the mantle observed in both body and surface waves, with significantly lower velocities observed beneath the Pacific plate in both the fast lid and the low velocity zone (Forsyth et al., 1998a,b; Gu et al., 2005; Hammond and Toomey, 2003; Harmon et al., 2009; Toomey et al., 1998; Weeraratne et al., 2007). On the Pacific plate, beneath the Sojourn and Hotu Matua volcanic chains, shear velocities are lower than the surrounding mantle to a depth of at least 150 km as determined from Rayleigh waves (Weeraratne et al., 2007) and with late (slow) P wave arrivals observed at stations within the free air anomaly (FAA) gravity lows (Harmon et al., 2007). The very low shear velocities observed in the seismic models have been attributed to increased temperatures beneath the Pacific plate and the presence of partial melt in the mantle (Forsyth et al., 1998a,b; Gu et al., 2005; Hammond and Toomey, 2003; Harmon et al., 2007, 2009; Toomey et al., 1998; Weeraratne et al., 2007). Seismic azimuthal anisotropy measurements from SKS splitting show fast directions that are roughly parallel to the direction of plate motion for the Pacific and Nazca plates, with 1 s split times observed on the Nazca plate (Wolfe and Solomon, 1998) and >5 Ma seafloor on the Pacific plate (Harmon

et al., 2004), and 2 s split times on the 0–5 Ma Pacific plate (Harmon et al., 2004; Wolfe and Solomon, 1998). The same pattern of variation in the magnitude of anisotropy across the axis and on older Pacific seafloor has been observed in 16–40 s period Rayleigh wave anisotropy, suggesting that the variation in the strength of anisotropy and by inference the pattern of mantle flow, is probably in the upper 100 km of the mantle (Harmon et al., 2009).

The geochemistry along strike of the southern EPR and the off axis volcanism on <10 Ma seafloor on the Pacific plate shows evidence for an enriched mantle component relative to normal mid ocean ridge basalt (NMORB). Particularly striking along axis for the longest ridge segment is a dramatic increase in $^3\text{He}/^4\text{He}$ ratio at 17°S, and a broad regional high from 16 to 20°S in $^{87}\text{Sr}/^{86}\text{Sr}$, $^{206}\text{Pb}/^{204}\text{Pb}$ ratios and a regional decrease in ϵNd , suggesting mixing of deeper mantle inputs from either the Easter (to the south) or Marquesas (west) hotspot into the ridge (Kurz et al., 2005; Mahoney et al., 1994). Off axis volcanism in the Rano Rahi seamounts and Puka Puka ridges show significantly increasing $^{87}\text{Sr}/^{86}\text{Sr}$, $^{206}\text{Pb}/^{204}\text{Pb}$ ratios, and decreasing ϵNd with increasing age of seafloor on which they were erupted, suggesting mixing with an increasingly enriched component from the Superswell region (Janney et al., 2000). Heavy rare earth element data indicate relatively shallow melting relative to plume fed hotspots with increased depth of melting to the west (Janney et al., 2000). Unpublished data from the Sojourn and Hotu Matua seamounts also suggest the lavas that make up the seamounts are the result of relatively shallow melting of isotopically enriched material with similarities to the Easter hotspot (Donnelly et al., 2003). All of the observations suggest that there is a fundamental difference between the mantle beneath the Pacific plate and the Nazca plate, and that there is some along-strike variability that is associated with the formation of these linear volcanic chains on the Pacific plate.

Observations of asymmetric subsidence, seamount production, geochemical and seismic heterogeneity have been explained by passive models in which there is a west-to-east thermal gradient in the deeper mantle with higher temperatures beneath the Pacific plate (Cochran, 1986) and westward migration of the ridge axis over a passively upwelling mantle containing relatively easily melted heterogeneities that produce more abundant off-axis volcanism on the leading Pacific plate

(Scheirer et al., 1998; Wilson, 1992). The question remains whether or not this heterogeneous material is just embedded ubiquitously in the mantle (Katz, 2010; Scheirer et al., 1998; Wilson, 1992) or it originates as Pacific Superswell plume material that is rapidly driven back to the ridge by return flow (Conder et al., 2002; Phipps Morgan et al., 1995; Toomey et al., 2002; Weeraratne et al., 2003).

We explore the origin of the Sojourn, Hotu Matua and easternmost Puka Puka volcanic chains and their associated FAA on young (<10 Ma), anomalously subsiding Pacific lithosphere using seismic, bathymetry and gravity data from the Mantle Electromagnetic and Tomography (MELT) (Forsyth et al., 1998a) experiment and the Gravity Lineations Intraplate Melting Petrologic and Seismic Expedition (GLIMPSE) experiment. These two experiments were located near the East Pacific Rise at 12 to 18°S, deploying ocean bottom seismographs for 6 and 11 months respectively, and compiling nearly 100% bathymetric and gravimetric coverage over the major volcanic edifices in the region. We present an improved regional shear velocity model from Rayleigh wave tomography, which jointly inverts the MELT and GLIMPSE data sets and uses finite frequency kernels to improve lateral resolution. We also extend the analyses of the mantle density structure and dynamic topography of Harmon et al. (2006) to the MELT study region and the Rano Rahi seamounts and the easternmost Puka Puka ridges. With our improved shear velocity model, gravity and topography analyses, we synthesize previous findings with our own to investigate 3-D flow in the mantle beneath the Pacific plate driven by heterogeneity.

2. Gravity and topography analysis

2.1. Residual Mantle Bouguer anomaly and residual topography

The seafloor topography and free air gravity anomaly are produced by the superposition of seamount loading of the seafloor, the flexural response of the lithosphere to loading, and any subsurface loading, assuming lateral variations in the oceanic crustal density are small. At short wavelengths, the seafloor topography and FAA are dominated by the volcanic loading at the seafloor, which obscures smaller topographic and density anomalies due to dynamic behavior coming from greater depths. To examine possible density contributions to the free air gravity anomaly, and possible dynamic seafloor topography from mantle heterogeneity, we calculate two quantities, the residual Mantle Bouguer gravity anomaly (rMBA) and the residual topography. We define the residual Mantle Bouguer anomaly as the FAA corrected for subsidence with age and the gravity anomaly contributions from surface volcanic loading and crustal thickening associated plate flexure, which is in contrast to the usual Mantle Bouguer anomaly that assumes a

constant thickness crust. The residual topography is the seafloor topography corrected for subsidence with age and the effects of surface volcanic loading of seamount chains. We remove the subsidence with age trend in the gravity and bathymetry data assuming a polynomial of the form: $c_0 + c_1x + c_2\sqrt{x}$, where x is age and $c_0 - c_2$ are the estimated coefficients. We solve for the trend for each of the Pacific and Nazca plates. The rMBA provides a map of the gravity anomalies arising due to mantle density anomalies, while the residual topography provides a map of dynamic topography caused by the mantle density anomalies. We follow the method of Harmon et al. (2006) to calculate these maps, extending the analysis to the Rano Rahi seamounts, using the satellite FAA (Sandwell and Smith, 2009) and shipboard swath bathymetry (Forsyth et al., 2006; Scheirer et al., 1996) as our data (Fig. 2A, 2B). We refer the reader to the original work, Supplementary material Section 1, and Fig. 2C for more details.

2.2. Regional residual topography map

The residual topography represents dynamic topography due to subsurface loading. The dominant trend we see in Fig. 3B is topography swells beneath the Sojourn Ridge, Hotu Matua, and the Rano Rahi Seamounts with bathymetric lows in between oriented in the direction of plate motion. These swells have amplitudes of ~100 m above the background with a wavelength of ~200 km (Fig. 3B). The swell amplitudes are >150 m beneath the peaks of the largest seamounts.

The swell topography continuity varies across the Pacific plate. The swell beneath Sojourn is continuous along the length of the ridge system extending from the western edge of our mapped region to the East Pacific Rise. Similarly, the broad swell topography beneath the Rano Rahi seamounts extends westward from the East Pacific Rise at 17–18°S to the Puka Puka ridges. At the EPR this swell appears to bifurcate in another swell lineament that is aligned with the trend of Hotu Matua swell, but there is a hiatus in this swell lineament centered at 116°W. The swell topography does not appear to extend further westward from Hotu Matua.

The swell topography extends 100 km east of the EPR. The residual topography either falls off to a background value of ± 30 m or goes to a negative value. The region of the Nazca plate near 17–18°S on the EPR does maintain some swell topography, but decays to the background values at ~100 km from the ridge. This section of the EPR also has the highest residual topography for the entire segment.

The undulating swell topography is a robust feature of the original bathymetry and is not an artifact of our processing. The strongest evidence for this is in regions with smaller seamount loads such as the Rano Rahi seamount field, which do not flex the plate significantly but have strong swell lineaments. In these regions, we have only

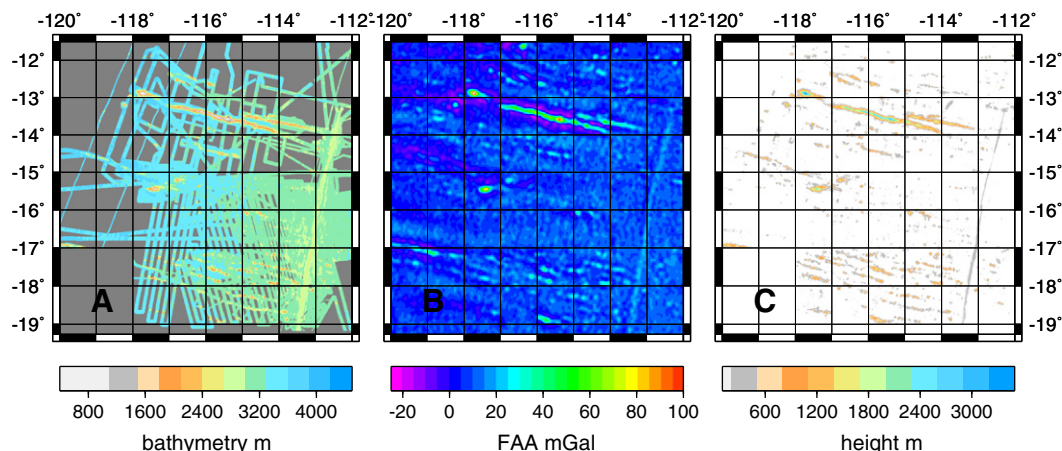


Fig. 2. (A) Swath bathymetry, (B) satellite Free Air gravity anomaly, and (C) isolated seamount load for the study region.

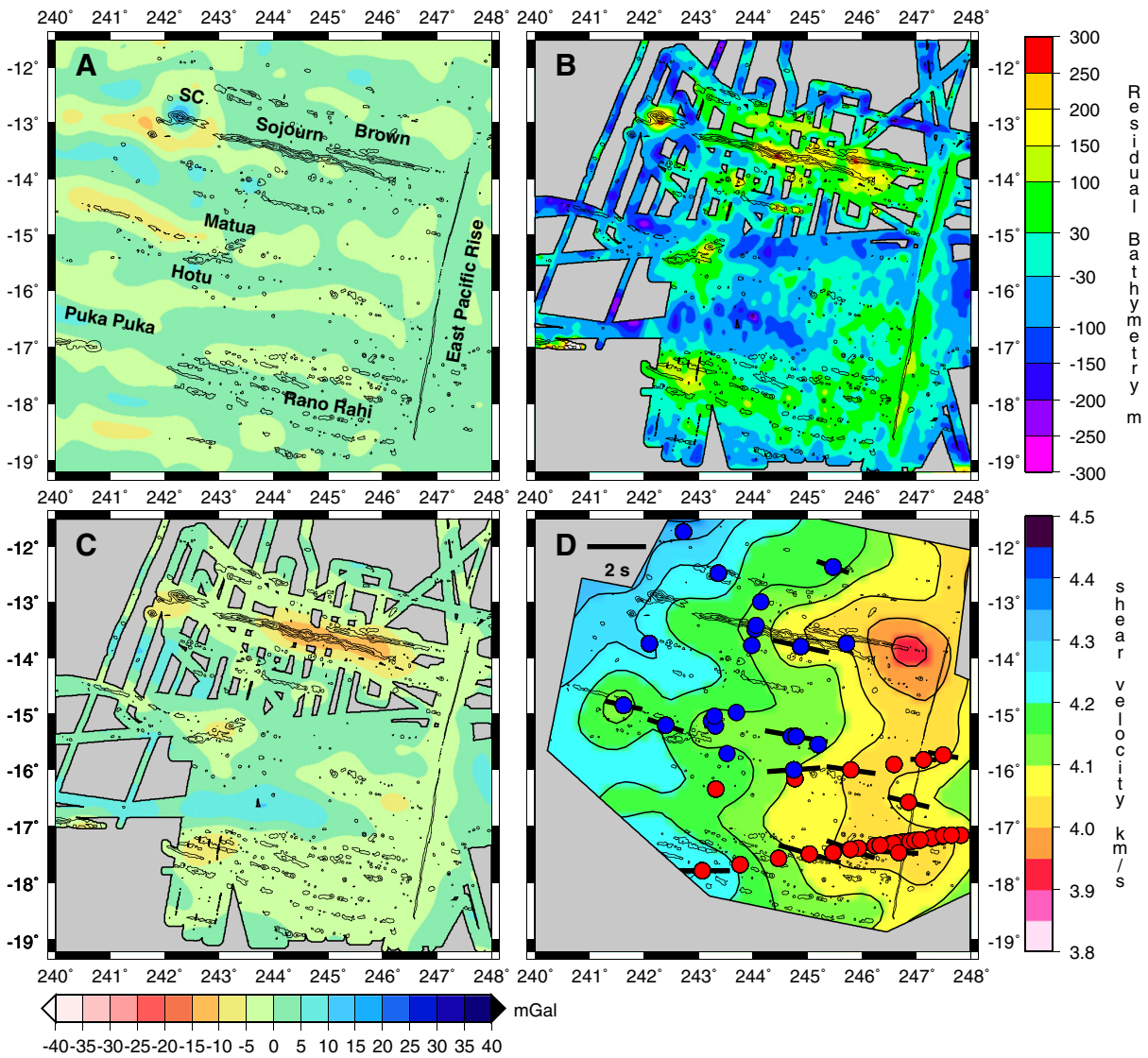


Fig. 3. The maps of (A) age detrended free air anomaly, (B) residual bathymetry, (C) residual Mantle Bouguer anomaly and (D) shear velocity (10–100 km depth) illustrate the spatial correlations between all four and the volcanic edifices in the region shown in black 800 m contours. The gray masked areas in B and C indicate regions where there is no bathymetric control within 5 km. The unmasked region in D shows where the seismic velocities are well constrained. Symbols in D show station locations of the MELT and GLIMPSE seismic deployments in the region: red circles are the MELT stations, blue circles are GLIMPSE stations. Vectors indicate the magnitude and direction of SKS splitting in the region. In all maps, except the shear velocity map, a linear and square root of age trend has been removed from the anomalies. SC in A is Southern Cross seamount.

removed the subsidence with age trend and the seamount load, so the undulation of the seafloor of the same age is highlighted.

2.3. Residual Mantle Bouguer anomaly (rMBA) map

The rMBA is due to density anomalies arising from mantle sources or crustal underplating or thinning, assuming small lateral variation in crustal density. The features in the rMBA map shown in Fig. 3C parallel the features observed in the residual topography. The largest anomalies visible are the ~200 km wavelength banded pattern with a strike roughly perpendicular to the ridge axis on the Pacific plate. The amplitude of these bands is 5–10 mGal. Low gravity anomalies are located beneath the major seamount chains (Hotu Matua, Rano Rahi/Puka Puka, and Sojourn).

The rMBA lineaments extend across the region from the west and truncate near the EPR. For the Sojourn and Rano Rahi groups, the gravity anomaly lows are continuous across the Pacific plate while the Hotu Matua low is discontinuous, with a gap at 116°W longitude. In the

western portion of the map, where there is little seamount loading, the rMBA is equal to the lows visible in the free air anomaly (Fig. 3A). On the Nazca plate, the rMBA goes to positive values within 50 km of the EPR.

The rMBA lows near the EPR on the Pacific plate show that the residual topography swells are compensated features. The compensation is also evident in the free air gravity anomaly, which is nearly zero near the EPR after we have removed the trend with age. This is particularly apparent in the region of the Rano Rahi seamount field.

Our choice of ~4 km effective elastic thickness for estimating the effects of flexural loading by the seamount chains, based on the average of the best fitting independent estimates of thickness from the individual volcanic edifices (Harmon et al., 2006) and density structure, affects the amplitudes of the observed patterns in both the rMBA and residual topography. However, for a reasonable range of effective elastic thicknesses, these features are robust and cannot be eliminated. For instance, decreasing the effective elastic thickness to 2 km creates stronger swell topography over the peaks of the edifices due to more local compensation

with positive peaks up to 300 m. The pattern in the rMBA is nearly the same, within ± 3 mGals of the rMBA shown in Fig. 3C. In addition, there may be some error in the rMBA caused by lateral density heterogeneity within the crust or by unaccounted for variations in crustal thickness or underplating. Except for the seamount edifices themselves, variations in crustal thickness along a 350-km-long north–south refraction profile across the Sojourn Ridge and the Hotu-Matua trend found less than 400 m variation in crustal thickness, not enough to explain the gravity anomalies (Holmes et al., 2007).

The presence of gravity lows and swells beneath the volcanic chains suggests that there is buoyant low-density material beneath the edifices in the mantle. We interpret the residual topography and rMBA anomalies as being due to mantle density anomalies due to the strong correlation of these anomalies with the seismic anomalies presented in Section 3. We discuss the geodynamic implications of this interpretation along with the implications of our seismic results in Section 4.

3. Rayleigh wave tomography

3.1. Rayleigh wave phase velocity and 3-D shear velocity inversion methods

We performed Rayleigh wave phase velocity tomography using the method of Forsyth and Li (2005) as modified by Yang and Forsyth (2006), which accounts for deviations from great circle path propagation of Rayleigh waves using a 2 plane wave approximation for each incoming wavefield and accounts for scattering of Rayleigh waves by velocity heterogeneities using 2-D finite frequency kernels. The inversion for shear velocity is a two-step process. Initially, we invert amplitude and phase data at each period to generate phase velocity maps, and then invert local phase velocity dispersion curves at each location in the phase velocity maps for shear velocity structure, producing a 3-D shear velocity model. The nodal parameterization for the phase velocity inversion and earthquakes are shown in Fig. 4, and the starting shear velocity model and example shear velocity

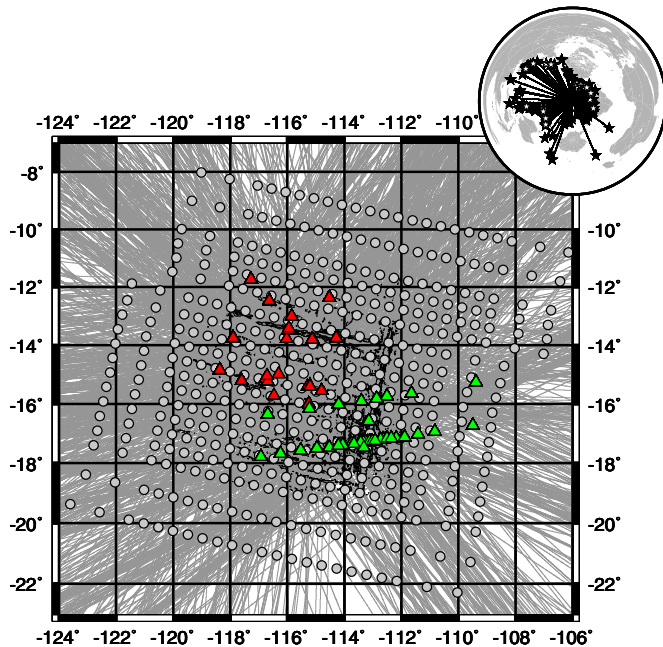


Fig. 4. Map of MELT station locations (green triangles), GLIMPSE station locations (red triangles), and node parameterization (gray circles). Gray lines show ray path coverage. Inset map shows earthquake locations (white MELT, black GLIMPSE events).

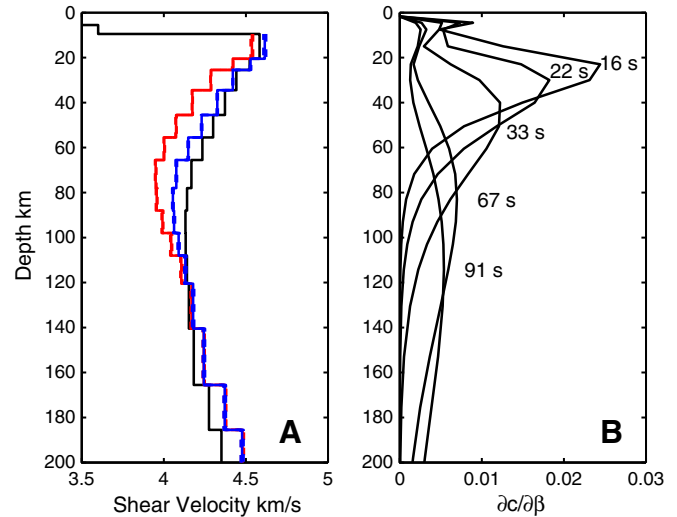


Fig. 5. (A) 1-D shear velocity starting model and two velocity profiles from -117.9° longitude and -13.75° latitude (blue—representing fast region between Hotu Matua and Sojourn Ridge) and -118.33° longitude, and -114.85° latitude (red—representing slow region beneath west of Hotu Matua). (B) Phase velocity sensitivity kernels to shear wave velocity for 16, 22, 33, 67 and 91 s period.

model outputs and sensitivity kernels we used for the shear velocity inversion are shown in Fig. 5. We refer the reader to Forsyth and Li (2005) and Yang and Forsyth (2006) and the Supplementary material Section 2 for more information about the method.

3.2. Phase velocity maps

We present 2-D phase velocity maps in Fig. 6 at selected periods. In these inversions we use a starting model that is the best fitting phase velocity as a function of age (Harmon et al., 2009). The velocity models are clipped using the approximate contour of the 2σ error of 0.05 km/s at our best-resolved period shown in Fig. 6 (22 s).

We observe a velocity gradient with increasing distance from the EPR in the phase velocity maps at the shortest periods of 16–22 s, with the lowest velocities at the EPR, which is also visible in inversions that have a uniform starting model. There are two focused zones of low velocities on the EPR in this period range, one at the eastern end of the Sojourn ridge system at 14° S, and another zone centered at 18° S, with higher velocities in between. The phase velocities along the spreading center are very low; at 16 s, the lowest on-axis velocities are <3.5 km/s, resulting in a 6–8% velocity decrease relative to the average velocity for the region.

In this period range, phase velocities at the three major volcano chains, Sojourn, Hotu Matua, and Rano Rahi, are lower than normal seafloor of similar age. This is particularly apparent in the 22 s period phase velocity map, where the velocity gradient from the EPR to the west has a finger-like pattern, with low velocities extending out beneath the trends of the three ridge systems, and higher velocity “fingers” extending in towards the ridge. The wavelength of these low velocity regions is approximately 200 km. The Rano Rahi finger is broadened relative to the Hotu Matua or Sojourn. These low velocity regions appear to extend to the western edge of the map. This pattern of low velocities beneath the Sojourn and Hotu Matua lines persists through the longer periods (25–50 s).

At longer periods, (25–50 s), the regional velocity low is located west of the EPR axis. The largest velocity lows are focused under the eastern end of the Sojourn ridge approximately 100 km west of the EPR. There is also a broad off axis velocity low in this period range approximately 100 km west of the EPR at 17° S. We also note that at 40–50 s period range there is a small velocity low east of the EPR beneath the Nazca plate at 17° S.

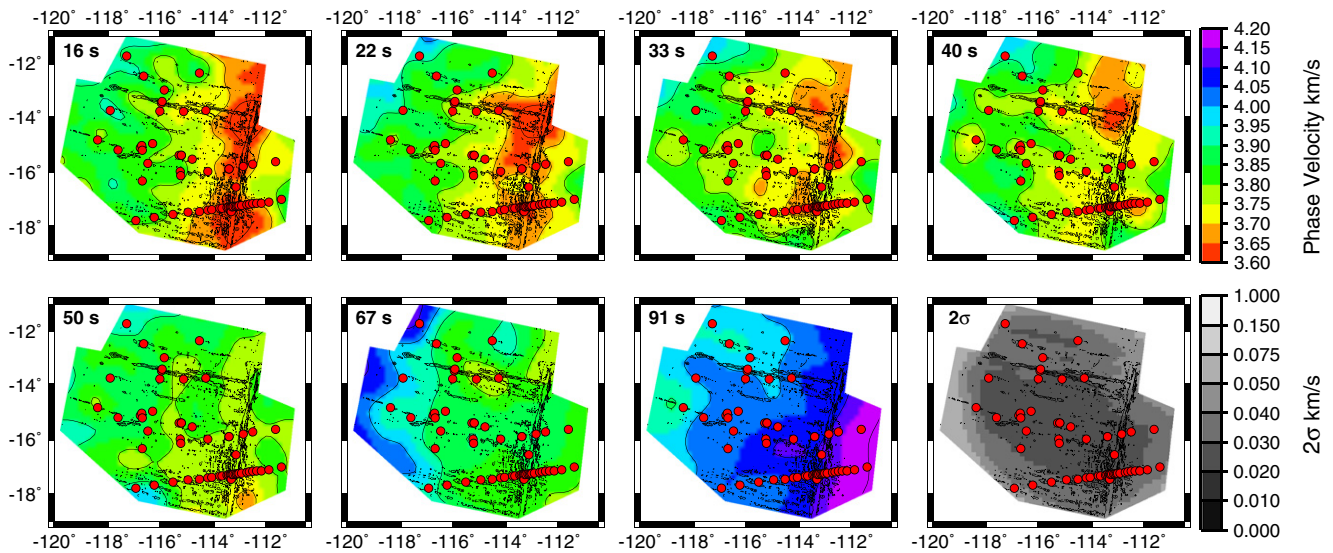


Fig. 6. Rayleigh wave phase velocity maps for 16, 22, 33, 40, 50, 67, and 91 s period, and 2σ standard error for 22 s period. Red circles are station locations and 1000 m contours show volcanic edifice locations.

We observe low velocity regions beneath the center of the Sojourner ridge system and beneath the Rano Rahi seamount chain for periods >67 s. These anomalies are broader and lower amplitude (1% anomaly) than at shorter periods. At the longer periods, >67 s, the resolution decreases, and although our models show velocity gradients with respect to distance from the EPR, they are not well resolved and do not appear in inversions in which the starting model is laterally uniform in phase velocity.

To describe the resolution of our models, we present the diagonals of formal resolution matrix, resolution length and anomaly amplitude bias (after Barmin et al., 2001) for the phase velocity map at 22 s period in Fig. 7A, B and C respectively. The formal resolution within the region is generally very good, with typical values of about 0.6 per node on a 0.5° grid, indicating that typically about 2 nodal values would have to be averaged to yield one well-resolved piece of information about the lateral velocity variation, Resolution lengths within most of the array are less than 150 km, suggesting that the 200 km wavelength features we observe are robust. The anomaly amplitude bias is the percentage difference between the input and output anomalies including the effects from adjacent nodes. The anomaly amplitude bias shows that the amplitudes recovered are typically within $\pm 5\%$ of the input anomaly, however in some regions, particularly near the Garrett fracture zone and the nearby EPR, this formal analysis indicates amplitudes of the velocity

anomalies may be 20% weaker than the true velocity anomaly. However, the formal analysis can be misleading, especially outside the arrays, because it only considers uncertainties assuming that the parameterized part of the world is the only source of variation. Delays from outside the model realm can map into the model realm to some extent and those effects will tend to be concentrated in poorly constrained parts of the model. So waves that are delayed propagating down the EPR might amplify the apparent anomaly in the vicinity of the Garrett/EPR intersection near the edge of our model area.

3.3. 3-D shear velocity model

We present the 3-D shear velocity model as a series of 3 depth averages, which are depth ranges that are well resolved according to the formal resolution analysis in our shear velocity inversion. This provides the minimum structure for interpretation, and we are confident in the features we observe. The depth averages are 10–45 km, 30–75 km, and 60–175 km depth and are shown in separate panels in Fig. 8.

The main feature observed in the 3-D shear velocity structure at the shallowest depths (10–45 km) is a strong gradient in velocity with distance from the ridge, which corresponds to increasing thickness of a high velocity lid reaching a maximum of about 45–50 km at 10 Ma (Harmon et al., 2009). The lowest shear velocities are found at

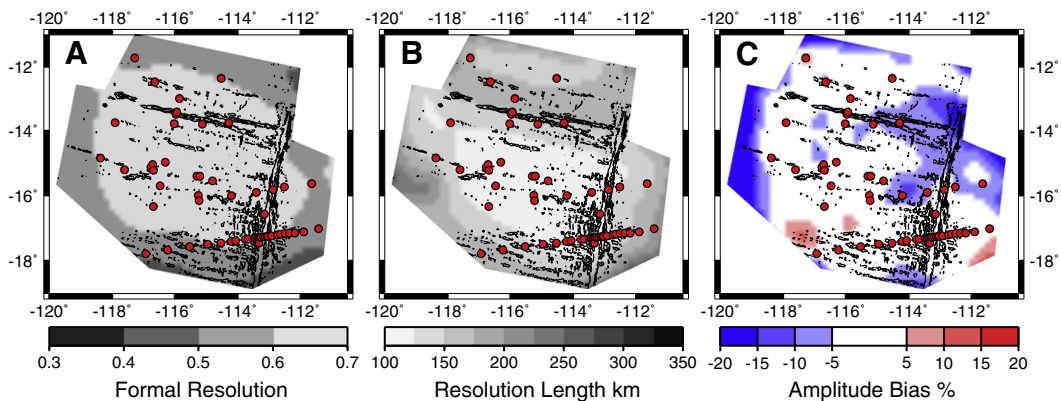


Fig. 7. For 22 s period, A) formal resolution matrix diagonal values for velocity parameters, B) resolution length for velocity parameters, and C) anomaly amplitude bias. Red circles indicate station locations; black lines 1000 m bathymetry contours.

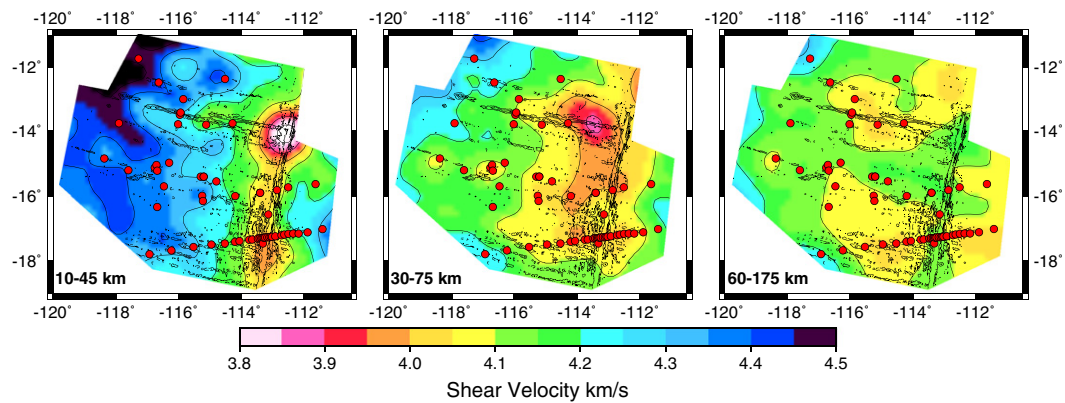


Fig. 8. Shear velocity model resolved depth averages for 10–45 km, 30–75 km, and 60–175 km depths. Red circles are station locations and 1000 m contours show volcanic edifice locations.

the ridge, with a minimum velocity of 3.76 km/s, increasing to just over 4.55 km/s at the western edge of the map. Along most of the ridge axis, velocities are 3.95–4.00 km/s in agreement with previous studies of the East Pacific Rise. The lowest velocities mapped are at the intersection of the Sojourn Ridge and the EPR. It should be noted that this location is outside both the MELT and GLIMPSE arrays. Although crossing rays and broad finite frequency response kernels provide some control on velocities outside the array, it is likely that the magnitude of the velocity anomaly is not well constrained, based on the formal amplitude anomaly bias for the phase velocity inversions presented in Fig. 7C. There is another low velocity region beneath the ridge at 18°S on the EPR.

There is a low velocity zone beneath the high velocity lid across the entire region in the 30–75 km and 60–175 km depth average. The velocities are on average 3% slower in the 30–75 km depth average than the 10–45 km depth average. The 60–175 km depth average velocity is 4% slower than the shallowest depth average. The lateral gradients are also smaller in this depth range, with maximum velocities of 4.39 km/s and a minimum velocity of 3.88 km/s.

In the 30–75 km depth average, the lowest velocities in the region are located ~100 km west of the EPR axis in an elongated region parallel to the EPR. The velocity increases in both directions perpendicular to the strike of the EPR axis. The strongest low velocity anomalies are centered beneath the Brown ridge and extending to the easternmost Sojourn ridge. At greater depths (60–175 km) the off axis low velocity region persists, but splits into two anomalies, one in the north, located beneath the Sojourn ridge system, and one in the south, with the lowest velocities beneath the Rano Rahi seamount field.

Relative to lithosphere of the same age, the velocity is slower beneath the length of the Sojourn, Hotu Matua and Rano Rani lines at all depths in a region about ~100 km wide. At 10–45 km depth, these lower velocities can be seen as a smaller velocity gradient with distance from the EPR axis, with the anomalies beneath the EPR axis being connected to these reduced gradients. At 30–75 km there is a strong low velocity region beneath the eastern edge of Sojourn ridge, which extends westward continuously increasing in velocity with increasing distance from the EPR. Beneath the Hotu Matua ridge system, there are isolated zones of low velocity directly beneath the edifices, and another small low velocity zone ~200 km west of the Hotu Matua volcanic complex. There is a small extension of the off-axis low velocity zone westward beneath the northern Rano Rahi. Relative to the surrounding seafloor, the velocities beneath the intraplate volcanic chains can be up to 3% lower. Deeper, the low velocity zones beneath seamount chains become less focused, broadening, although some of the lack of focus may be attributed to reduced horizontal resolution caused by increased wavelengths and decreased numbers of observations at the longer periods that are sensitive to greater depths.

3.4. Comparison of shear velocity model to rMBA and residual topography

We highlight several features that are spatially coincident between the rMBA, residual topography and our shear velocity model averaged over 10–100 km depth (Fig. 3B, C, D). First, beneath Sojourn Ridge, there is good agreement between the location of the low velocity region, the rMBA gravity low and the swell topography. In all three data sets the anomaly exists near the EPR axis and extends beneath the length of the Sojourn system to the Southern Cross seamount. Immediately south of Sojourn, the velocities increase, while the rMBA become positive and the residual topography becomes negative. Near Hotu Mata, we see a discontinuous anomaly beneath the volcanic complex in the shear velocity model, the rMBA, and residual topography. Finally, we see a broadened seismic low velocity anomaly west of the EPR at 17–18°S, where the trends of the Hotu Matua and Rano Rahi chains converge.

The low velocities in the shear velocity model at 30–75 km depth are not well correlated with the gravity and topography data at the southernmost edge of the Rano Rahi seamount chain. Here the shear velocity model is near the background average, while the rMBA is negative and there is significant swell topography. The correlation improves in this area at greater depth in the shear velocity model (60–175 km), when the shear velocity low beneath the Rano Rahi broadens to include most of the seamount field.

4. Discussion

4.1. Interpretation of seismic and marine geophysical results

The low gravity anomalies and swell topography indicate low-density buoyant material exists beneath the volcanic ridges in the region. The 5–10 mGal rMBA anomalies require a density contrast of 20–50 kg/m³ assuming density variation occurs over a large depth range, e.g., the upper 40–100 km of the mantle. In addition, the lowest velocities beneath the Pacific plate are 5–7% slower than the surrounding mantle within the resolution of our study. The correlation of the rMBA lows and residual topography swells with low seismic velocities beneath the volcanic edifices in the 30–175 km depth averages suggests that some of these density anomalies are located at asthenospheric depths and are not due solely to crustal underplating.

A combination of increased temperature and subsequent melt retention can explain the observed asthenospheric low density and seismic velocity anomalies beneath the volcanic chains. A purely thermal explanation does not work because a ~200 °C thermal anomaly, assuming a coefficient of thermal expansion of $3 \times 10^{-5} \text{ K}^{-1}$, can account for the density anomaly, but produces only a 1–2% velocity anomaly using either the partial derivative of shear modulus with respect to temperature (Schutt and Lesher, 2006) or the parameterization of Stixrude and

Lithgow-Bertelloni (2005) with anelastic effects included (e.g. Harmon et al., 2009). Alternately, 4% melt volume assuming melt density of 2800 kg/m³ could produce the density anomaly, but would result in too great a reduction in shear velocity, given 7.9% shear velocity reduction for 1% melt fraction (Hammond and Humphreys, 2000). Using a linear combination of melt and temperature, we estimate that to simultaneously fit the seismic and gravity data we require a thermal anomaly of ~150 °C with 0.5–0.6% retained melt. These estimates are in line with the thermal anomaly required to explain the asymmetry in subsidence in the Pacific in the region (Cochran, 1986), thinning of the elastic lithosphere beneath the seamounts (Goodwillie, 1995; Harmon et al., 2006), thinning of the seismically fast lid (this study, Weeraratne et al., 2007) body wave delays (Harmon et al., 2007), and recent estimates for equilibrium silicate-carbonate melt fractions of over 0.3% in the asthenosphere beneath 0–10 Ma seafloor (Hirschmann, 2010). A thermal anomaly and partial melt might also explain the increase in the magnitude of seismic azimuthal anisotropy on 0–5 Ma Pacific seafloor (Fig. 3D, Harmon et al., 2004; Wolfe and Solomon, 1998); a temperature increase of ~100 °C can increase the strain rate of dislocation creep by an order of magnitude due to its Arrhenius temperature relationship, while <1% partial melt can increase the strain rate of the mantle by one to two orders of magnitude relative to a dry melt-free mantle (Faul and Jackson, 2007).

We do not favor other mechanisms such as mantle depletion or water as a crystallographic defect in olivine to explain the seismic and gravity anomalies. Water as a crystallographic defect in olivine cannot produce density anomalies, and the resistivity data suggest that the uppermost 60 km of the upper mantle region is dry (Baba et al., 2006a,b; Evans et al., 2005), so we do not think that enhanced water content is directly responsible for the anomalies we observe. However, enhanced water content may help to lower the viscosity of the mantle, enhancing flow (Hirth and Kohlstedt, 1996) and aid in mantle melting in the region, especially if water is heterogeneously distributed in the mantle. Bulk composition is expected to have a small effect on density and seismic velocity in the upper 67 km of the mantle, e.g. 20% depletion is required to produce 0.42–0.46% density decrease (~15 kg/m³) (Schutt and Leshner, 2006). We expect that the range of depletion is much smaller in the upper mantle especially off-axis after it has been melted at the EPR.

4.2. Implications for geodynamic models

The low densities and seismic velocities indicate that the thermal structure in general is hotter beneath the Pacific plate than beneath the Nazca plate. Beneath the Pacific plate the thermal structure varies laterally, with higher temperatures and melt fractions beneath the intraplate volcanic ridges. The lateral variation in temperature is not predicted by simple half-space cooling models and therefore requires dynamic behavior, upwelling hotter mantle material beneath the intraplate volcanic ridges in the asthenosphere.

Thermal contraction and cracking of the lithosphere have been suggested to explain the linear seamount chains and the free air gravity anomaly (Cormier et al., 2011; Gans et al., 2003; Sandwell and Fialko, 2004), but this process does not predict the observed anomalies in the sub-lithospheric mantle. These models also predict residual topography lows beneath the seamount chains caused by downward flexure of the crack walls and normal fault scarps. Forsyth et al. (2006) did not observe normal faulting perpendicular to the spreading center in the region, while Harmon et al. (2006) and this study found topography highs beneath the seamount chains after correcting for the downward flexure under the weight of the seamounts. In addition, the gravity anomalies and seismic anomalies presented in this study and previous studies are at odds with a purely lithospheric process. Diffuse lithospheric extension (Sandwell et al., 1995), has been ruled out because there is no evidence for increased spacing of fracture zones on lithosphere of increasing age (Gans et al., 2003; Goodwillie, 1995; Neumann and Zuber, 1994). Cracking of the lithosphere may be

necessary to tap the melt generated in the asthenosphere to create the linear seamount chains (e.g. Sandwell et al., 1995) but does not provide a means of generating the melt in the first place and would preferentially remove melt from the asthenosphere beneath the seamount chains, producing high velocity anomalies rather than the low velocity anomalies that are observed.

Purely thermally driven small-scale convection (Ballmer et al., 2009; Buck and Parmentier, 1986; Korenaga and Jordan, 2003; Richter and Parsons, 1975) does not explain all of our and previous observations of the Pacific plate in our study region. First, thermal small-scale convection requires several million years to generate convective instabilities (Ballmer et al., 2009; Buck and Parmentier, 1986; Korenaga and Jordan, 2003; Richter and Parsons, 1975), and therefore cannot explain our observations of seismic and density anomalies that extend to zero age lithosphere. Edge driven convection (King and Anderson, 1998), due to juxtaposition of older lithosphere with zero age lithosphere at the Garrett fracture zone might explain the volcanism at Sojourn. However, this becomes less likely in the case of the Hotu Matua and Rano Rahi trends, which are not located near fracture zones. Second, the purely thermal small scale convection models do not explain the enriched mantle mixing trend of the intraplate volcanism and along axis variation on the EPR (Janney et al., 2000; Kurz et al., 2005; Mahoney et al., 1994) other than through melting of preexisting entrained, enriched plume material (Ballmer et al., 2010). Finally, the thermally driven small-scale convection model should be applicable to both the Pacific and Nazca plates, thus not explaining the marked asymmetry in subsidence, seamount production, seismic structure and the termination of anomalies on the Nazca plate side within 100 km of the EPR in our study region.

However, mantle heterogeneity can create small-scale convection on young seafloor through melt buoyancy effects rather than through thermal instabilities (e.g. Hernlund et al., 2008; Katz, 2010; Raddick et al., 2002; Tackley and Stevenson, 1993) providing a better explanation of our observations. Off axis melt buoyancy driven mantle flow may arise in a homogenous mantle at fast spreading rates (Barnouin-Jha et al., 1997), but variable melting of heterogeneous mantle material aids the efficiency of the process and can explain the geochemical trends. Instabilities from heterogeneities could arise beneath the thermal boundary layer if large-scale mantle convection of a heterogeneous mantle, viscous fingering or return flow beneath a thinning plate causes upwelling and increased melting of more fertile mantle (schematic shown in Fig. 9). Higher degrees of melting on the Pacific plate side of the EPR of more fertile mantle could produce greater melt buoyancy effects adding to the asymmetric melting and subsidence beneath the westward migrating EPR at 17°S (Katz, 2010). These heterogeneities may be stretched out by the motion of the overriding plate and be organized into small-scale convection. Locally enhanced upwelling created by melt-enhanced buoyancy can produce both the thermal and melt anomalies we infer from our seismic and gravity data. We prefer melt buoyancy over depletion buoyancy because in the upper 67 km (2 GPa) the density difference due to depletion is relatively small (Schutt and Leshner, 2006) and thus is not expected to contribute significantly to upwelling.

The heterogeneous, enriched mantle material needed for our modified small-scale convection model could have a variety of sources. Isotopically, the heterogeneities represented in the off-axis lavas of the Puka-Puka, Rano-Rahi, Hotu-Matua and the Sojourn seamounts and ridges and in the along-strike variations on the EPR represent a mixture between an N-MORB source and a “C”-like endmember (Donnelly et al., 2003; Hall et al., 2006; Janney et al., 2000; Kurz et al., 2005; Mahoney et al., 1994). The C-type or “common” endmember is not very diagnostic, being found in many places in the South Pacific, including the Marquesas, Easter Island and the Tuamotus. Janney et al. (2000) and Hall et al. (2006), preferred an origin in the Superswell to the west based on west-to-east decrease in strength of the C endmember, easterly elongations of apparent C concentrations in the seamount basalts, and the paucity of seamounts on the Nazca plate to the east, but the heterogeneities could also be

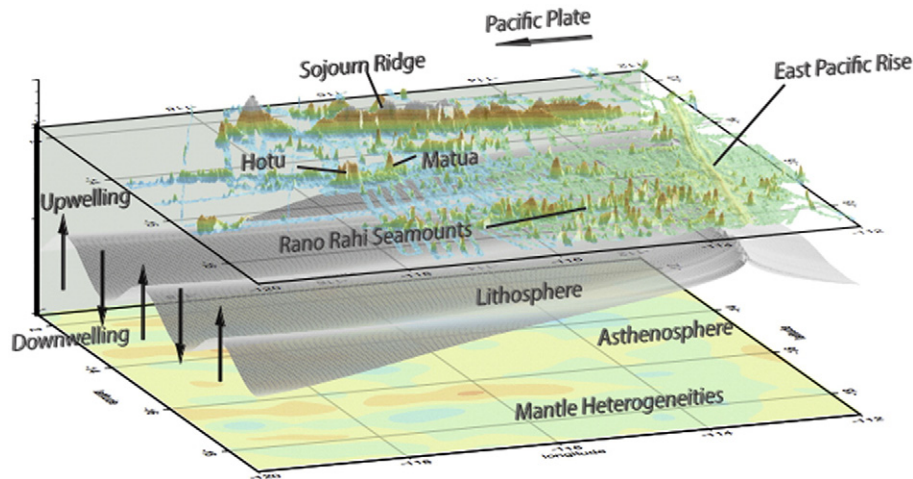


Fig. 9. Schematic model of mantle flow in the region. In our idealized model shown here, the lithosphere thickens by conductive cooling away from the spreading center and becomes more rigid. Mantle heterogeneities pulled up by the upwelling generated by the separating, thickening plates may result in enhanced melting off axis, triggering small-scale convection and further upwelling. Shear between the plate and the deeper mantle may elongate the heterogeneities and suppress small-scale convection aligned with the spreading center. Viscous fingering in return flow from the Pacific Superswell region from the west to East Pacific Rise could also elongate the heterogeneities. Near the mid ocean ridge, the plate is flexible enough to create swell topography above the heterogeneous melting regions. Above the upwelling regions, higher temperatures may locally thin the lithosphere further increasing flexibility of the lithosphere and local uplift.

ubiquitously, albeit irregularly, distributed in the Pacific mantle. Migration of the EPR to the west could preferentially melt the heterogeneities on the Pacific side of the EPR, a tendency that would be enhanced by return flow from the Superswell region to the EPR (Conder et al., 2002; Gaboret et al., 2003; Phipps Morgan et al., 1995; Toomey et al., 2002). Elongation of the heterogeneities could be generated either by shear between the Pacific plate and deeper mantle or by Saffman–Taylor instabilities (viscous fingering) in the return flow (Weeraratne et al., 2003).

Return flow from the Superswell is predicted from global models of mantle flow beneath the Pacific, with significantly higher azimuthal anisotropy at all ages of the Pacific plate relative to the Nazca plate (Gaboret et al., 2003), while SKS splitting measurements in the region decrease to the same magnitude as the Nazca plate (1 s split times) on >5 Ma Pacific plate seafloor (Harmon et al., 2004; Wolfe and Solomon, 1998). With small scale convection in the return flow, we expect a decrease in azimuthal anisotropy with increasing seafloor age as small-scale convection flow disrupts the laminar flow caused by the overriding plate (Hall et al., 1999), in agreement with the observed anisotropy.

Heterogeneity induced small scale convection may also explain the short wavelength gravity lineaments observed near the axis on both the Pacific and Nazca plate at 5–10°S on the EPR (Fig. 1). In this region, heterogeneities may upwell beneath either side of the axis and be organized by the overriding plate. Farther off-axis, thermally driven small-scale convection may explain the banded pattern observed in the FAA across the Pacific basin (Fig. 1) especially in the central Pacific away from the Superswell region.

The implication of this work is the pattern of mantle convection in the region is more complicated than passive upwelling driven by plate spreading and conductive cooling of the lithosphere away from the ridge. We have shown there is an active component of upwelling off-axis beneath the intraplate seamounts, which has changed the thermal structure of the lithosphere and asthenosphere. Many uncertainties remain that could be resolved by examining the structure beneath the gravity lineaments in regions not affected by seamount topography, to test for the presence of swell topography, low seismic velocities and changes in resistivity at depth. Additional measurements of seismic anisotropy in these regions would help to better constrain mantle flow at depth.

5. Conclusions

We show that beneath three volcanic intraplate seamount chains and their associated free air gravity lineaments there are low shear

velocities, topographic swells and low-density anomalies in the mantle that extend to zero age seafloor. In addition, we show that beneath the anomalously subsiding Pacific plate there is an elongated region of low seismic velocity parallel to the EPR centered 100 km off axis in the shallowest asthenosphere. The correlation between the seismic velocity anomalies at 30–175 km depth and the rMBA suggests that some part of the gravity lineament anomaly is due to density anomalies in this depth range. We interpret the seismic and density anomalies in the asthenosphere as arising from the combined effects of a small thermal anomaly (<150 °C) and <0.6% retained melt.

To generate the gravity lineaments and intraplate volcanic ridges, we prefer a model in which small-scale convection is triggered by heterogeneity in the mantle rather than by instability of the lower lithosphere. Purely lithospheric processes such as thermal bending and cracking models do not predict thermal anomalies in the asthenosphere, so we rule out this family of models as being the dominant mechanism producing the linear volcanic chains and gravity anomalies.

Appendix A. Supplementary data

Supplementary data to this article can be found online at doi:10.1016/j.epsl.2011.09.038.

References

- Baba, K., Chave, A.D., Evans, R.L., Hirth, G., Mackie, R.L., 2006a. Mantle dynamics beneath the East Pacific Rise at 17 degrees S: insights from the Mantle Electromagnetic and Tomography (MELT) experiment. *J. Geophys. Res.* 111. doi:10.1029/12004JB003598.
- Baba, K., Tarits, P., Chave, A.D., Evans, R.L., Hirth, G., Mackie, R.L., 2006b. Electrical structure beneath the northern MELT line on the East Pacific Rise at 15 degrees 45' S. *Geophys. Res. Lett.* 33. doi:10.1029/2006GL027528.
- Ballmer, M.D., van Hunen, J., Ito, G., Bianco, T.A., Tackley, P.J., 2009. Intraplate volcanism with complex age-distance patterns: a case for small-scale sublithospheric convection. *Geochim. Geophys. Geosyst.* 10, Q06015. doi:10.1029/2009GC002386.
- Ballmer, M.D., Ito, G., van Hunen, J., Tackley, P.J., 2010. Small-scale sublithospheric convection reconciles geochemistry and geochronology of intraplate volcanoes in the western and southern Pacific. *Earth Planet. Sci. Lett.* 290, 224–232.
- Barmin, M.P., Ritzwoller, M.H., Levshin, A.L., 2001. A fast and reliable method for surface wave tomography. *Pure Appl. Geophys.* 158, 1351–1375.
- Barnouin-Jha, K., Parmentier, E.M., Sparks, D.W., 1997. Buoyant mantle upwelling and crustal production at oceanic spreading centers: on-axis segmentation and off-axis melting. *J. Geophys. Res.* 102, 11979–11989.
- Buck, W.R., Parmentier, E.M., 1986. Convection beneath young oceanic lithosphere; implications for thermal structure and gravity. *J. Geophys. Res.* 91, 1961–1974.
- Cochran, J.R., 1986. Variations in subsidence rates along intermediate and fast spreading midocean ridges. *Geophys. J. R. Astron. Soc.* 87, 421–454.

- Conder, J.A., Forsyth, D.W., Parmentier, E.M., 2002. Asthenospheric flow and asymmetry of the East Pacific Rise. *J. Geophys. Res.* 107, 2344.
- Cormier, M.H., Gans, K.D., Wilson, D.S., 2011. Gravity lineaments of the Cocos Plate: evidence for a thermal contraction crack origin. *Geochem. Geophys. Geosyst.* 12, Q07707. doi:10.1029/2011GC003573.
- Donnelly, K., Langmuir, C.H., Goldstein, S.L., 2003. Geochemical constraints on melting process in the GLIMPSE region. *Eos Trans. Am. Geophys. Union*, Fall Meeting Suppl. p. 84. V21B-05.
- Evans, R.L., Hirth, G., Baba, K., Forsyth, D., Chave, A., Mackie, R., 2005. Geophysical evidence from the MELT area for compositional controls on oceanic plates. *Nature* 437, 249–252.
- Faul, U.H., Jackson, I., 2007. Diffusion creep of dry, melt-free olivine. *J. Geophys. Res. Solid Earth* 112, B04204. doi:10.1029/2006JB004586.
- Forsyth, D.W., Li, A., 2005. Array-analysis of two-dimensional variations in surface wave phase velocity and azimuthal anisotropy in the presence of multipathing interference. In: Levander, A., Nolet, G. (Eds.), *Seismic Data Analysis and Imaging with Global and Local Arrays* (AGU Monograph).
- Forsyth, D.W., Scheirer, D.S., Webb, S.C., Dorman, L.M., Orcutt, J.A., Harding, A.J., Blackman, D.K., Phipps, M.J., Detrick, R.S., Shen, Y., Wolfe, C.J., Canales, J.P., Toomey, D.R., Sheehan, A.F., Solomon, S.C., Wilcock, W.S.D., Melt Seismic Team, U.S., 1998a. Imaging the deep seismic structure beneath a mid-ocean ridge: the MELT experiment. *Science* 280, 1215–1218.
- Forsyth, D.W., Webb, S.C., Dorman, L.M., Shen, Y., 1998b. Phase velocities of Rayleigh waves in the MELT experiment on the East Pacific Rise. *Science* 280, 1235–1238.
- Forsyth, D.W., Harmon, N., Scheirer, D.S., Duncan, R.A., 2006. Distribution of recent volcanism and the morphology of seamounts and ridges in the GLIMPSE study area: implications for the lithospheric cracking hypothesis for the origin of intraplate non hotspot volcanic chains. *J. Geophys. Res.* 111, B11407. doi:10.1029/2005JB004075.
- Gaboret, C., Forte, A.M., Montagner, J.P., 2003. The unique dynamics of the Pacific Hemisphere mantle and its signature on seismic anisotropy. *Earth Planet. Sci. Lett.* 208, 219–233.
- Gans, K.D., Wilson, D.S., Macdonald, K.C., 2003. Pacific plate gravity lineaments: diffuse extension or thermal contraction? *Geochem. Geophys. Geosyst.* 4, 1074. doi:10.1029/2002GC000465.
- Goodwillie, A.M., 1995. Short-wavelength gravity lineations and unusual flexure results at the Puka Puka volcanic ridge system. *Earth Planet. Sci. Lett.* 136, 297–314.
- Gu, Y.J., Webb, S.C., Lerner-Lam, A., Gaherty, J.B., 2005. Upper mantle structure beneath the eastern Pacific Ocean ridges. *J. Geophys. Res. Solid Earth* 110, B06305. doi:10.1029/2004JB003381.
- Hall, C.E., Parmentier, E.M., Fisher, K.M., 1999. Is there an anisotropic signature of small-scale convection in the Pacific upper mantle? *Eos, Transactions, American Geophysical Union*, Fall Meeting Suppl. p. 80. Abstract S41D-05.
- Hall, L.S., Mahoney, J.J., Sinton, J.M., Duncan, R.A., 2006. Spatial and temporal distribution of a C-like asthenospheric component in the Rano Rahi Seamount Field, East Pacific Rise, 15 degrees–19 degrees S. *Geochem. Geophys. Geosyst.* 7, Q03009. doi:10.1029/2005GC000994.
- Hammond, W.C., Humphreys, E.D., 2000. Upper mantle seismic wave velocity: effects of realistic partial melt geometries. *J. Geophys. Res.* 105, 10975–10986.
- Hammond, W.C., Toomey, D.R., 2003. Seismic velocity anisotropy and heterogeneity beneath the Mantle Electromagnetic and Tomography Experiment (MELT) region of the East Pacific Rise from analysis of P and S body waves. *J. Geophys. Res. Solid Earth* 108.
- Harmon, N., Forsyth, D.W., Fischer, K.M., Webb, S.C., 2004. Variations in shear-wave splitting in young Pacific seafloor. *Geophys. Res. Lett.* 31. doi:10.1029/2004GL020495.
- Harmon, N., Forsyth, D.W., Scheirer, D.S., 2006. Analysis of gravity and topography in the GLIMPSE study region: isostatic compensation and uplift of the Sojourn and Hotu Matua Ridge systems. *J. Geophys. Res.* 111, B11406. doi:10.1029/2005JB004071.
- Harmon, N., Forsyth, D.W., Lamm, R., Webb, S., 2007. P and S delays beneath intraplate volcanic ridges and gravity lineations near the East Pacific Rise. *J. Geophys. Res.* 112. doi:10.1029/2006JB004392.
- Harmon, N., Forsyth, D.W., Weeraratne, D.S., 2009. Thickening of young Pacific lithosphere from high-resolution Rayleigh wave tomography: a test of the conductive cooling model. *Earth Planet. Sci. Lett.* 278, 96–106.
- Haxby, W.F., Weissel, J.K., 1986. Evidence for small-scale mantle convection from Seasat altimeter data. *J. Geophys. Res.* 91, 3507–3520.
- Hernlund, J.W., Tackley, P.J., Stevenson, D.J., 2008. Buoyant melting instabilities beneath extending lithosphere: 1. Numerical models. *J. Geophys. Res.* 113, B04405. doi:10.1029/2006JB004862.
- Hirschmann, M.M., 2010. Partial melt in the oceanic low velocity zone. *Phys. Earth Planet. Inter.* 179, 60–71.
- Hirth, G., Kohlstedt, D.L., 1996. Water in the oceanic upper mantle; implications for rheology, melt extraction and the evolution of the lithosphere. *Earth Planet. Sci. Lett.* 144, 93–108.
- Holmes, R.C., Webb, S.C., Forsyth, D.W., 2007. Crustal structure beneath the gravity lineations in the Gravity Lineations, Intraplate Melting, Petrologic and Seismic Expedition (GLIMPSE) study area from seismic refraction data. *J. Geophys. Res.* 112. doi:10.1029/2006JB004685.
- Janney, P.E., Macdougall, J.D., Natland, J.H., Lynch, M.A., 2000. Geochemical evidence from the Pukapuka volcanic ridge system for a shallow enriched mantle domain beneath the South Pacific Superswell. *Earth Planet. Sci. Lett.* 181, 47–60.
- Katz, R.F., 2010. Porosity-driven convection and asymmetry beneath mid-ocean ridges. *Geochem. Geophys. Geosyst.* 11. doi:10.1029/2010GC003282.
- King, S.D., Anderson, D.L., 1998. Edge-driven convection. *Earth Planet. Sci. Lett.* 160, 289–296.
- Korenaga, J., Jordan, T.H., 2003. Linear stability of Richter rolls. *Geophys. Res. Lett.* 30. doi:10.1029/2003GL018337.
- Kurz, M.D., Moreira, M., Curtice, J., Dempsey, E.L., Mahoney, J.J., Sinton, J.M., 2005. Correlated helium, neon, and melt production on the super-fast spreading East Pacific Rise near 17°S. *Earth Planet. Sci. Lett.* 232, 125–142.
- Mahoney, J.J., Sinton, J.M., Kurz, M.D., Macdougall, J.D., Spencer, K.J., Lugmair, G.W., 1994. Isotope and trace element characteristics of a super-fast spreading ridge: East Pacific Rise, 13–23°S. *Earth Planet. Sci. Lett.* 121, 173–193.
- Marquart, G., Schmeling, H., Braun, A., 1999. Small-scale instabilities below the cooling oceanic lithosphere. *Geophys. J. Int.* 138, 655–666.
- Neumann, G.A., Zuber, M.T., 1994. Modeling constraints on diffuse extension on the Pacific Plate. *Eos, Transactions, American Geophysical Union*, 75, p. 590.
- Phipps Morgan, J., Morgan, W.J., Zhang, Y.-S., Smith, W.H.F., 1995. Observational hints for a plume fed, suboceanic asthenosphere and its role in mantle convection. *J. Geophys. Res.* 100, 12 (753–712,767).
- Raddick, M.J., Parmentier, E.M., Scheirer, D.S., 2002. Buoyant decompression melting: a possible mechanism for intraplate volcanism. *J. Geophys. Res.* 107, B2228. doi:10.1029/2001JB000617.
- Richter, F.M., Parsons, B., 1975. On the interaction of two scales of convection in the mantle. *J. Geophys. Res.* 80, 2529–2541.
- Sandwell, D.T., Fialko, Y., 2004. Warping and cracking of the Pacific plate by thermal contraction. *J. Geophys. Res.* 109, B10411. doi:10.1029/2004JB0030912004.
- Sandwell, D.T., Smith, W.H.F., 2009. Global marine gravity from retracked Geosat and ERS-1 altimetry: ridge segmentation versus spreading rate. *J. Geophys. Res.* 114, B01411. doi:10.1029/2008JB006008.
- Sandwell, D.T., Winterer, E.L., Mammertick, J., Duncan, R.A., Lynch, M.A., Levitt, D.A., Johnson, C.L., 1995. Evidence for diffuse extension of the Pacific Plate from Pukapuka ridges and cross-grain gravity lineations. *J. Geophys. Res.* 100, 15 (087–015,099).
- Scheirer, D.S., Macdonald, K.C., Forsyth, D.W., Miller, S.P., Wright, D.J., Cormier, M.H., Weiland, C.M., 1996. A map series of the Southern East Pacific Rise and its flanks, 15 degrees S to 19 degrees S. *Mar. Geophys. Res.* 18, 1–12.
- Scheirer, D.S., Forsyth, D.W., Cormier, M.H., Macdonald, K.C., 1998. Shipboard geological indications of asymmetry and melt production beneath the East Pacific Rise near the MELT experiment. *Science* 280, 1221–1224.
- Schutt, D.L., Leshar, C.E., 2006. Effects of melt depletion on the density and seismic velocity of garnet and spinel lherzolite. *J. Geophys. Res. Solid Earth* 111. doi:10.1029/2003JB002950.
- Stixrude, L., Lithgow-Bertelloni, C., 2005. Mineralogy and elasticity of the oceanic upper mantle: origin of the low-velocity zone. *J. Geophys. Res.* 110, B03204 (03210.01029/2004JB002965).
- Tackley, P.J., Stevenson, D.J., 1993. A mechanism for spontaneous self-perpetuating volcanism on the terrestrial planets. In: Stone, D., Runcorn, S.K. (Eds.), *Flow and Creep in the Solar Systems: Observations, Modeling and Theory*. Kluwer, Netherlands, pp. 307–321.
- Toomey, D.R., Wilcock, W.S., Solomon, S.C., Hammond, W.C., Orcutt, J.A., 1998. Mantle seismic structure beneath the MELT region of the East Pacific Rise from P and S wave tomography. *Science* 280, 1224–1227.
- Toomey, D.R., Wilcock, W.S.D., Conder, J.A., Forsyth, D.W., Blundy, J.D., Parmentier, E.M., Hammond, W.C., 2002. Asymmetric mantle dynamics in the MELT region of the East Pacific Rise. *Earth Planet. Sci. Lett.* 200, 287–295.
- Weeraratne, D., Parmentier, E.M., Forsyth, D.W., 2003. Viscous fingering of miscible fluids in laboratory experiments and the oceanic mantle asthenosphere. *Eos, Transactions, American Geophysical Union*, Fall Meeting Suppl. p. 84. Abstract V21B-03.
- Weeraratne, D.S., Forsyth, D.W., Yang, Y., Webb, S.C., 2007. Rayleigh wave tomography beneath intraplate volcanic ridges in the South Pacific. *J. Geophys. Res.* 112, B06303. doi:10.1029/2006JB00440.
- White, S.C., Umino, S., Kumagia, H., 2006. Transition from seamount chain to intraplate volcanic ridge at the East Pacific Rise. *Geology* 34, 293–296.
- Wilson, D.S., 1992. Focused mantle upwelling beneath midocean ridges – evidence from seamount formation and isostatic compensation of topography. *Earth Planet. Sci. Lett.* 113, 41–55.
- Winterer, E.L., Sandwell, D.T., 1987. Evidence from en-echelon cross-grain ridges for tensional cracks in the Pacific Plate. *Nature (London)* 329, 534–537.
- Wolfe, C.J., Solomon, S.C., 1998. Shear-wave splitting and implications for mantle flow beneath the MELT region of the East Pacific Rise. *Science* 280, 1230–1232.
- Yang, Y., Forsyth, D.W., 2006. Regional tomographic inversion of amplitude and phase of Rayleigh waves with 2-D sensitivity kernels. *Geophys. J. Int.* 166, 1148–1160.